Three-dimensional nanotub submicrometer diffraction gratings for solar cells

Cyrus Ho, Josephine McKeon, Daniel Macdonald, and Kylie R. Catchpole*

Research School of Engineering, Australian National University, ACT 0200, Australia

*Corresponding author: kylie.catchpole@anu.edu.au

Received 25 June 2014; revised 28 August 2014; accepted 4 September 2014;
posted 4 September 2014 (Doc. ID 214555); published 9 October 2014

Diffraction gratings are a promising approach for reducing reflection and achieving light-trapping in solar cells. Using square lattices as a base structure, we investigate a novel bi-periodic nanotub three-dimensional grating structure and compare it with established textured structures for thin-film and wafer applications. For wafer application, simulations show that optimal AR coated nanotubs demonstrated solar weighted reflectance (SWR) of 2% compared to AR coated square pyramids with values 1.9%. Nanotubs also show SWR below 8% for polar angles to 60°. Simulated short-circuit current thin-film cells with nanotubs using smaller dimensions show higher yields (3–6 mA/cm^2 average) compared to square pyramids. For periods greater than 700 nm at aspect ratios of 0.7 and greater, nanotubs have reduced current attributed to the increased planar surface area of the nanotub base, and evident in increased SWR. A simple nanoimprint lithography process was employed in experiments to define a square array of circular holes, utilizing a polydimethylsiloxane (PDMS) stamp applied onto a sol–gel imprint resist. The underlying silicon was then wet etched to produce the nanotub textures of 200 nm height and 513 nm period. AR coated nanotub wafers were produced via plasma enhanced chemical vapor deposition (PECVD), with an experimental and theoretical SWR of 6.4% and 5.4%, respectively.

OCIS codes: (220.4241) Nanostructure fabrication; (050.6624) Subwavelength structures; (310.1210) Antireflection coatings; (240.0310) Thin films; (050.0050) Diffraction and gratings; (050.1950) Diffraction gratings.

http://dx.doi.org/10.1364/AO.53.006840

1. Introduction

Diffraction gratings can reduce reflection and trap light in solar cells, potentially increasing the efficiency and reducing the material cost of photovoltaics by employing thinner wafers. The optical path is elongated for the incident light, which is coupled to high diffraction orders [1], reducing transmittance and increasing the path length of light within the solar cell. Absorption enhancement of shorter wavelengths is attributed to an antireflection effect. Longer wavelengths involve a combination of anti reflection and light trapping [2].

Structures that provide a gradual change in refractive index are promising because they can lead to low reflectance via impedance matching. By manipulating the dimensions and profile of the texture, the effective refractive index is altered along with surface reflectance experienced [3].

Enhancement of photon absorption via light confinement has previously been investigated with a variety of submicrometer diffractive structures. Symmetrical textured structures of pyramids, pillars, and checkerboard grids have been assessed by Chong *et al.* and Mellor *et al.*, identifying optimized structures for current performance and highlighting square pyramids as superior to others [2,4]. Sai *et al.* and Abouelsaood *et al.* assessed square pyramids similarly, with an increased emphasis on the effects of aspect ratios, sizing, shape, and packing density on reflectance [5,6]. Textures mimicking naturally occurring structures of tapered profiles such as the moth-eye and dome formations were

1559-128X/14/296840-06$15.00/0

investigated by Sun *et al.*, Boden *et al.*, and Zhou *et al.* and optimized for antireflection demonstrating competitive current values [7–9].

Therefore, a sunken tapered profile is potentially promising for light trapping and antireflection. In this paper, nanotubs, a sunken dome etched into the silicon surface with and without silicon nitride AR coating, is investigated. The shape nanotub is based on an oblate hemispheroid (i.e., with its radius in general different from its height) resembling a washbasin. The tapered edges of the structure allow reduction in reflection from the silicon surface. We show that light trapping and antireflection for this structure is comparable to square pyramids, and we present experimental results on structures fabricated with nanolithography.

2. Methods

The optical performance of the nanotub's structure was modeled numerically using rigorous coupled wave analysis (RCWA) with a thin crystalline silicon substrate thickness of 3 μm, and short-circuit current (J_{sc}) was calculated by integrating the absorptance over the solar spectrum. The nanotub's structure was then optimized via current output and trends were plotted for a range of aspect ratios (0.1–1) for grating periods. To identify the effect of the texturing on solar weighted reflectance (SWR) in simulations, the substrate thickness was set to infinite (representing a wafer based solar cell for wavelengths up to around 1000 nm), with a layer of silicon nitride as an AR coating. Nanoimprinting based on substrate conformal imprint lithography (SCIL) [10] was performed to produce the nanotub's structure on silicon wafers, followed by etching and deposition of silicon nitride via plasma enhanced chemical vapor deposition (PECVD). Reflectance of the resulting wafers was measured with a spectrophotometer with integrating sphere.

A. Simulation

RCWA was performed with MATLAB and GD-Calc software [11]. The grating period was varied in the range 200–1000 nm, and height was varied within the range 200–1000 nm. The range for the incident wavelength of light used in the simulations is 400–1100 nm. Solar spectral irradiance data (photon flux at AM1.5G) equivalent to an irradiance of 100 mW/cm^2 was used [12] Optical data for silicon and silicon nitride were obtained from the literature [13]. For normal incidence, simulations were performed with TE polarized light as the symmetrical bi-periodic structures do not vary with polarization. For the analysis of the oblique angles an average of TE and TM polarization values were taken for both the short-circuit current and reflectance.

GDCalc generates transmission and reflection efficiencies that can be used to calculate the absorptance:

$$A = 1 - \left[\sum_m R_m + \sum_m T_m\right],$$

where A is the absorptance, and R_m and T_m are reflectance and transmittance for the given diffracted orders.

Current was obtained by integrating the absorptance over the solar photon flux (assuming all generated electron–hole pairs are collected), yielding J_{sc} [4],

$$J_{sc} = \int_{400}^{1100} (A(\lambda) q \Phi(\lambda) \mathrm{d}\lambda)$$

q is the value for the electronic charge and Φ is the photon flux as a function of wavelength λ.

SWR is given as [14]

$$\mathrm{SWR} = \frac{\int \Phi(\lambda) R(\lambda) \mathrm{d}\lambda}{\int \Phi(\lambda) \mathrm{d}\lambda},$$

$R(\lambda)$ is the wavelength-dependent reflectance.

Grating structures were created in GDCalc based on stratums, as illustrated in Fig. 1 where each stripe and block established periods and shapes. Structures were formed by having a set number of stratums at very small thicknesses where the number of stratums was determined by convergence tests. The J_{sc} produced demonstrated that 15 stratums were sufficient for grating construction as variance was within 0.1 mA/cm^2. The number of diffraction orders was also chosen based on convergence tests. Current stabilized with 0.5 mA/cm^2 variance for four diffraction orders for tests run. To balance accuracy and simulation time, five diffracted orders were chosen for the simulations.

Simulations were done on two types of substrates of silicon: finite and infinite thickness. The substrate with finite thickness was set to 3 μm (representing a thin-film silicon solar cell) with the superstrata having the permittivity of air. Structures were also set to be symmetric, with equal grating periods in the x and y directions. Pyramids were selected as an e stablished structure for comparing with nanotub structures. Pyramid structures were modeled by having strata that varied in dimensions equally in

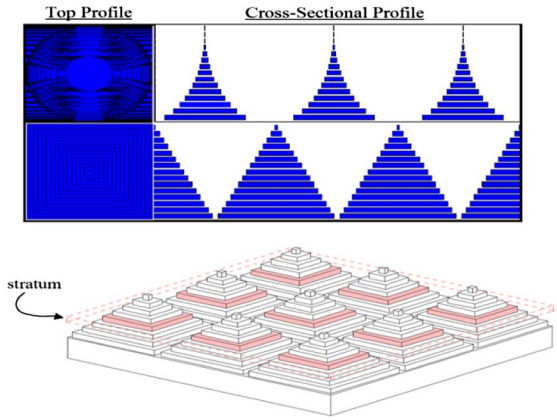

Fig. 1. Construction of diffraction grating, consisting of a substrate layered on top with a specified number of stratums. Blue represents the etched silicon and white represents air.

the x and y axes. Nanotub structures were created using trigonometrical functions to produce a hemispheroidal shape as illustrated in the cross-section in Fig. 1. Packing density was set to 100% for all structures. Infinite thickness was set to obtain the SWR, a measure that is particularly important for wafer-based solar cells.

B. Experimental Method and Process

The textures of nanotubs were fabricated experimentally on silicon wafers using a variant of nanoimprinting called SCIL. This method consists of the following steps: (1) formation of the sol–gel resist coating; (2) imprinting sol–gel imprint resist with a flexible, patterned polydimethylsiloxane (PDMS) stamp and curing. The PDMS stamp used here consists of a square array of cylindrical pillars of 51 3 nm period and 200 nm in height in 100% packing density, which creates cylindrical holes in the imprinted resist; (3) wet etching to remove the residual layer of sol–gel resist (usually around 10 nm in thickness) and to isotropically etch the underlying silicon, forming a nanotub shape.

The sol–gel imprint resist is made up of the following chemicals: methyl-tri-methoxy-silane (MTMS), tetra-methyl-ortho-silicate (TMOS), formic acid, N-propanol and 1,2-propanediol. The first stage of preparing the SiO_2 sol–gel resist is the hydrolysis stage. This is done by mixing 1:1:1 molar ratio of TMOS, MTMS, and n-propanol together. Water is added to the mixture above to a H_2O/Si molar ratio of around three to four where alcohol condensation is favored. Then, formic acid is added to the solution to acidify the solution to a pH of around 2 to speed up the hydrolysis process. The solution is placed in a water bath in room temperature to hydrolyze for 20 min. Later, 30 times the original ratio of TMOS and MTMS of n-propanol is added to the solution to make sure that there is excess alcohol, along with water to increase the H_2O/Si molar ratio to favor water condensation. The solution is let to mix for another 20 min. Finally, equal amounts of n-propanol, which contains 2 weight percent of 1,2-propandiol, are mixed with the solution made previously to increase the viscosity of the solution for spinning. The sol–gel imprint resist was then applied to the wafer, which was first dipped in hydrofluoric acid (HF) and dried in N_2. The sol–gel was spin-coated in an enclosed spinner (a modified Laurel Technologies Spinner, Model WS65OSZ-6NPP/Lite). The PDMS imprint stamp was applied within seconds while the sample was wet with coating and held *in situ* to dry at room temperature for 4 h for curing. The use of PDMS for the stamp allows volatile components of the imprint resist evaporating through the stamp. The stamp was removed, creating cylindrical holes of 513 nm period and 200 nm height, where the wafer was heated to 75°C for 20 min and annealed in nitrogen gas at 400°C for 20 min, increasing the density of the layer for etching. The wafer was etched, using tweezers to hold, in a mixture of acetic acid, H_3PO_4, HNO_3, and HF in the ratio of 30:25:3:0.5 for 5 min with gentle agitation. The acetic and H_3PO_4 served as buffers for introducing higher viscosity to the solution for a more even etch, HF and HNO_3 in the ratio stated provided smoothness for the surface profile via limited diffusion reaction [15,16]. The timing for the isotropic etch of the cylindrical imprints into nanotubs, as well as the ratio of acids for etching, was based on several iterations and observation. The sample was then removed from the solution and rinsed in deionized (DI) water. An HF dip was introduced to remove the remaining sol–gel and the wafer was then finally rinsed in DI water again and dried with an N_2 gun. Deposition of silicon nitride was done via PECVD for 3 min. As a result, an SiN thickness of 70 nm was produced.

3. Results and Discussion

A. Numerical Optimization of Thin Film Structure

Values of J_{sc} were calculated at 3 μm substrate thickness for varying grating period and height for nanotubs and pyramidal structures to determine optimal values. The results for the non-AR coated and AR coated structures are shown in Figs. 2 and 3, and the parameters for the optimal structures are given in Table 1. Aspect ratios 1 and 0.1 were omitted as the values did not vary and also to prevent reducing the resolution of the graph.

Optimized nanotubs and pyramidal structures based on current performance were obtained; current enhancement compared to the planar reference was 124% and 129%, respectively (Table 1). Pyramid structures yielded a slightly higher maximum current, while nanotub structures displayed higher current performance throughout a greater range of grating heights. In particular the nanotubs structures had higher-current performance at lower aspect ratios ranging from 0.2 to 0.4. This is important because the aspect ratio is often limited by

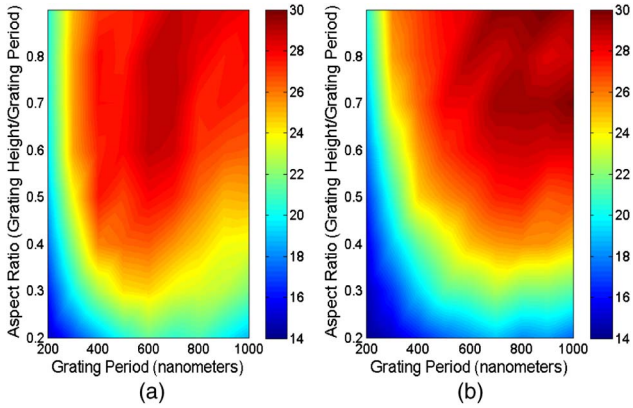

Fig. 2. Short circuit current density J_{sc} (mA/cm^2) of (a) nanotubs and (b) pyramids as a function of grating period and aspect ratio without nitride AR coating at a substrate thickness of 3 μm. Nanotubs have higher current at lower aspect ratios spanning 0.2–0.4.

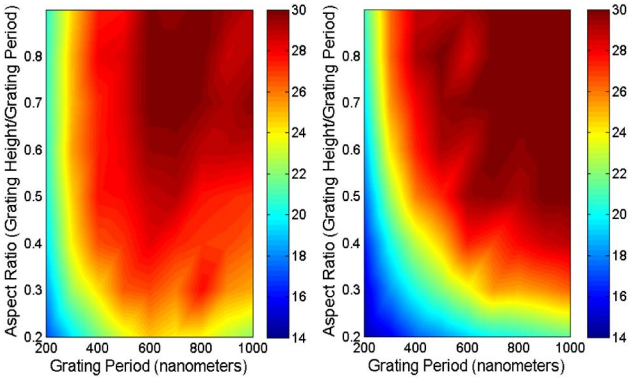

Fig. 3. Short-circuit current density J_{sc} (mA/cm^2) of (a) nanotubs and (b) pyramids as a function of grating period and aspect ratio with nitride AR coating at a substrate thickness of 3 μm. Nanotubs still have higher current at lower aspect ratios spanning 0.2–0.4, but lower maximum current performance.

fabrication techniques or material quality issues. The optimal aspect ratios for nanotubs and pyramid structures are 0.69 and 0.8, respectively. For the nanotubs structure [Figs. 2(a) and 3(a)] with aspect ratio less than or equal to 1, current was on average 3–6 mA/cm^2 higher than for the pyramidal structure [Figs. 2(b) and 3(b)] for grating periods 200–650 nm.

For a 3 μm thick cell (Table 2), AR coated optimal dimensions were 750 height 700 period (nanotubs) and 550 height 700 period (pyramids). Upon the application of the AR coating, compared to the square pyramids, the nanotubs saw a slightly higher increase in current, having a higher rise in highly absorbing regions (400–700 nm) indicated in the efficiency of AR coating on the surface profile; its

Table 1. Optimized Values for Diffraction Grating Structures for 3 μM Substrate Thickness Without AR Coating

Simulated Structures			
		Optimized Parameters	
Type	J_{sc} (mA/cm^2)	$d1 = d2$ (nm)	Height (nm)
Planar	13.1	—	—
Nanotub	29.4	650	450
Square pyramid	30.1	850	765

Table 2. Current Performance Without and With AR Coating, Showing Highly Absorbing (400–700 nm) and Weakly Absorbing (700–1100 nm) Regions

Current Without AR Coating (mA/cm^2)		
Spectral Wavelength (nm)	Nanotubs	Pyramids
Total	29.4	30.1
400–700	16.3	17.5
700–1100	13.1	12.6
Current with AR coating (mA/cm^2)		
Total	30.7	31.1
400–700	17.7	17.9
700–1100	12.9	13.2

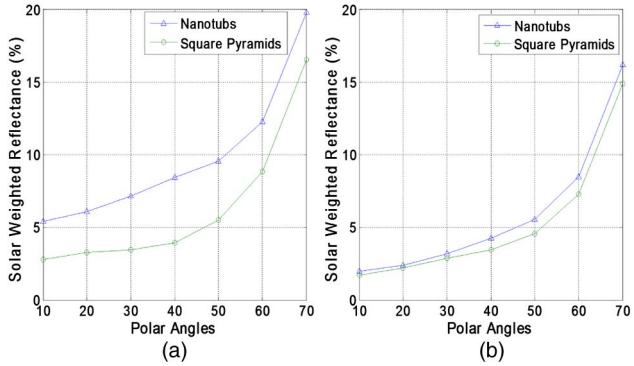

Fig. 4. SWR results for TE and TM averaged polar angles of incident light upon (a) non-AR coated and (b) AR coated cells.

light trapping efficiency however, (700–1100 nm) was overshadowed by the square pyramids.

When the angle of incidence was varied without an AR coating, pyramids performed better. However, with the application of AR coating [Figs. 4(a) and 4(b)], the nanotubs SWR for the range of polar angles were equivalent to the square pyramids.

B. Frontal Surface Reflectance, Transmittance and Current Performance

Optimal structures were assessed for the frontal surface reflectance, eliminating transmittance, and rear reflectance through the use of a semi-infinite substrate. The results are shown in Fig. 5, which also plots the wavelength dependence of the first to third diffraction order lines. For Figs. 6(a) and 6(b), aspect ratios 1 and 0.1 were omitted as the values did not vary and also to prevent reducing the resolution of the graphs.

The lowest reflectance (Fig. 5) was seen between the first and second diffraction orders; more incident light was able to couple into higher orders coinciding with increased absorptance in this region. Increased reflectance was observed past 400 nm grating periods for the high-energy part of the solar spectrum. However, the optimal grating period which produces

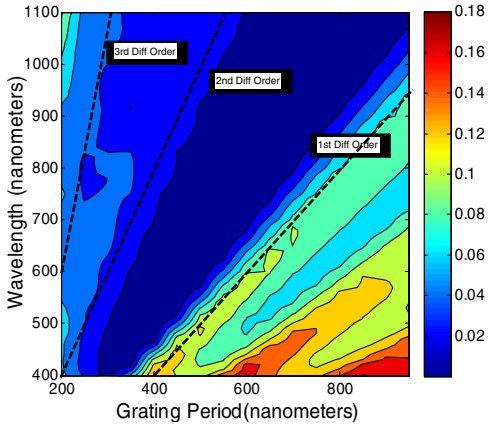

Fig. 5. Reflectance of nanotub structure without AR coating with aspect Ratio = 0.69. The first through third diffraction orders are also plotted indicating optimal light in-coupling between orders 1 and 2.

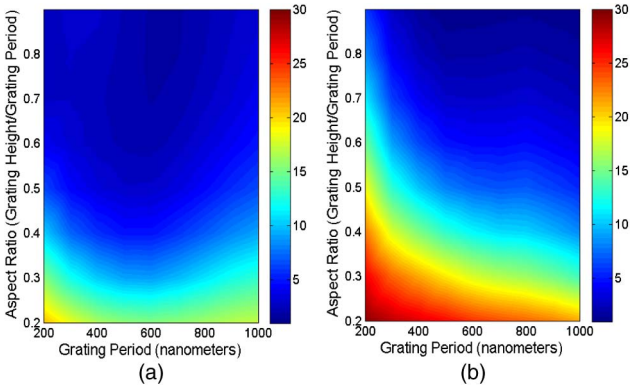

Fig. 6. Total SWR for nanotub and pyramid structures at aspect ratios for 200–950 nm periods with AR coating. Significantly lower reflectance could be observed for nanotubs with lower periods and high aspect ratios.

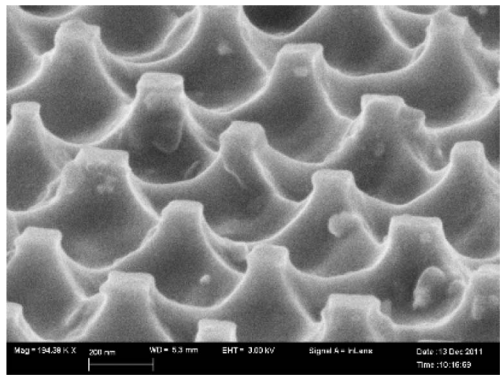

Fig. 7. SEM image of sample nanotubs 200 nm height and 51 3 nm in period.

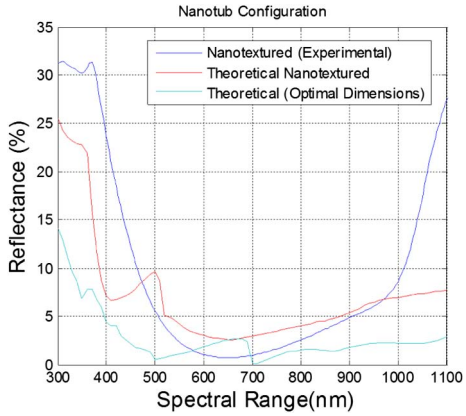

Fig. 8. Experimental and theoretical data with AR coating. The reflectance from the 900–1100 nm region is due to reflection from the rear of the wafer, which is not included in the simulated structure.

maximum current in thin cells is 650 nm, which indicates that for thin cells, both light trapping and reduced reflectance were important, in agreement with Chong *et al.* [2]. At the optimized aspect ratio for nanotubs (0.69) for finite thickness, high absorptance and low reflectance were obtained where $\lambda/d = 1$, similar to Mellor *et al.* where for circular pillars the region $0.9 < \lambda/d < 1.1$ μm had the best light trapping configuration for gratings [4].

Total SWR values [Fig. 6(b)] produced by symmetrical square pyramids showed similar trends to those seen by Sai *et al.* reduced by 5%–10% throughout due to the AR application [5]. Higher aspect ratios were necessary for both structures to have periods to minimize reflection losses. Nanotubs demonstrated superior antireflective values compared to values for pyramidal gratings for smaller dimensions (periods less than 700 nm and aspect ratios 0.1–0.7). Additionally, reduced reflectance in these ranges correlate with the increased current produced compared to the square pyramidal structure [Figs. 2(b) and 3(b)]. With periods greater than 700 nm however, it was observed that the increased base area of the nanotubs which acts as a planar surface reduces the effectiveness of the tapered profile of the height; increasing 3%–5% in reflectance for aspect ratios greater than 0.5. The tapered profile of the nanotubs, which gave a gradual change in effective refractive index via surface relief, increased performance and reduced reflectance for grating period ranges below 700 nm, corroborating with the theory of Southwell on the effects of the surface relief and its effective refractive index and reflectance [3]. Combined AR coating and surface texture resulted in optimal SWR of 2.0% for nanotubs and 1.9% for pyramids, respectively.

C. Experimental Results

SEM images of the textured structures dimensions of 513 nm period and 200 nm height are shown in Fig. 7. The instrument used to scan was an SEM Zeiss Ultra Plus Gemini. Reflectance measurements were done using a Perkin Elmer Lambda 1050 with integrating sphere.

Observable in the SEM images are minute defects produced in the etching process, fragments remaining in the wells, uneven surfaces, and overly etched corners. This was due to uneven coverage of imprint, which created the structural discrepancies observed in Fig. 7. Additionally, dendrite features of crystallized sol–gel imprint resist were observed, possibly through contact with air during the drying process after being spun in an enclosed spinner. The contact of air was primarily due to its introduction through the edges of the stamps while holding the sample *in situ*.

Table 3. Experimental and Simulated SWR for the As Fabricated Structures, along with the Simulated SWR of an Optimal Structure

Solar Weighted Reflectance (%)	
Experimental (200 height/513 nm period)	6.4
Simulated	
As fabricated (200 height/513 nm period)	5.4
Optimal (750 height/700 nm period)	2.0

The reflectance values observed from experiments and simulated structures with AR coating are displayed in Fig. 8. The deviations from the simulated spectrum are attributed to physical imperfections and overly etched walls, as seen in Fig. 7. As shown in Table 3, the simulated and nanotextured non-optimal structure with AR coating produced similar SWR. The experimental sample created (200 nm height 513 nm period, 0.38 aspect ratio) however, was not the optimal structure identified (750 nm height 700 nm period, 1.1 aspect ratio), having higher reflectance as observed in Table 3.

4. Conclusions

It was demonstrated in simulations that submicrometer nanotubs gave better SWR performance and increased current compared to square pyramidal structures. This was shown for periods 200–1000 nm at aspect ratios 0.1–1, where values of J_{sc} across range of dimensions for nanotubs structures were 3–6 mA/cm^2 higher and SWR decreased up to 15%. The SWR and current at those dimensions for the nanotubs was attributed to its tapered structure leading to impedance matching. Under varying polar angles of incident light with the application of AR coating, it was shown that the nanotub structure's SWR was also equivalent. However, relatively higher SWR was observed for structures with larger aspect ratios and grating period; the increase in planar surface area led to higher reflectance and lower current than the pyramids.

Experimentally, SWR of 6.4% was achieved using a nanoimprinting technique against the expected theoretical SWR of 5.4%, this was largely attributed to the slight over etching of the nanotub textures resulting in lowered walls. It is predicted that this could be reduced to 2.0% with an optimized structure that has a higher aspect ratio. The fabrication process described here provides flexibility as it could be applied to many types of solar cells in contrast to inverted pyramids, which are only applicable to single crystal silicon.

The authors are grateful to the Australian Research Council, the Australian Renewable Energy Agency, and Trina Solar for providing funding for this work.

References

1. P. Wurfel, *The Physics of Solar Cells* (Wiley, 2009)..
2. T. K. Chong, J. Wilson, S. Mokkapati, and K. R. Catchpole, "Optimal wavelength scale diffraction gratings for light trapping in solar cells," J. Opt. A **14**, 2–5 (2012).
3. W. H. Southwell, "Pyramid-array surface-relief structure producing antireflection index matching on optical surfaces," J. Opt. Soc. Am. A **8**, 549–553 (1991).
4. A. Mellor, I. Tobias, A. Marti, and A. Luque, "A numerical study of bi-periodic binary diffraction gratings for solar cell applications," Sol. Energy Mater. Sol. Cells **95**, 3527–3535 (2011).
5. H. Sai, Y. Kanamori, K. Arafune, Y. Ohshita, and M. Yamaguchi, "Light trapping effect of submicron surface textures in crystalline Si solar cells," in *Progress in Photovoltaics: Research and Applications* (Wiley, 2007), Vol. **15**, pp. 415–418.
6. A. A. Abouelsaood, S. A. El-Naggar, and M. Y. Ghannam, "Shape and size dependence of the anti-reflective and light trapping action of periodic grooves," in *Progress in Photovoltaics: Research and Applications* (Wiley, 2002), Vol. **10**, p. 513.
7. C.-H. Sun, P. Jiang, and B. Jiang, "Broadband moth-eye antireflection coatings on silicon," Appl. Phys. Lett. **92**, 061112 (2008).
8. S. A. Boden and D. M. Bagnall, "Optimization of moth-eye antireflection schemes for silicon solar cells," in *Progress in Photovoltaics: Research and Applications* (Wiley, 2010), Vol. **18**, p. 195.
9. W. Zhou, M. Tao, L. Chen, and H. Yang, "Microstructured surface design for omnidirectional antireflection coatings," J. Appl. Phys. **102**, 103105 (2007).
10. M. Verschuuren and H. van Sprang, "3D photonic structures by sol-gel imprint lithography," Mater. Res. Soc. Symp. Proc. **1002**, 1–3 (2007).
11. K. Johnson, http://software.kjinnovation.com/GD-Calc.html.
12. ASTMG173-03, Standard Tables for Reference Solar Spectral Irradiances: Direct Normal and Hemispherical on 37° Tilted Surface (ASTM International, 2005).
13. E. D. Palik, *Handbook of Optical Constants of Solids* (Academic, 1985).
14. J. Nelson, in *The Physics of Solar Cells* (Imperial College, 2003), pp. 54–88.
15. S. Franssila, *Introduction to Microfabrication* (Wiley, 2010), pp. 130–132.
16. D. Kendall and R. Shoultz, "Wet chemical etching of silicon and SiO_2, and ten challenges for micromachiners," in *Handbook of Microlithography, Micromachining and Microfabrication* (Institution of Engineering and Technology, 1997), pp. 41–97.